JSST
Journal of Space Science & Technology

Vol. 8/ No. 4/ 2015
pp. 19-27

Equilibrium Effects on the Hypersonic Laminar Boundary Layer Flow over Axisymmetric Bodies

R. Kamali Moghadam[1*] and M. R. Salimi[2]

1. Aerospace Research Institute, Ministry of Science, Research and Technology

2. Aerospace Engineering Department, Sharif University of Technology

Postal Code: 14665-834, Tehran, IRAN

rkamali@ari.ac.ir

An accurate and efficient computational procedure is developed to predict the laminar hypersonic flowfield for both the perfect gas and equilibrium air around the axisymmetric blunt body configurations. To produce this procedure, the boundary layer equations utilize the integral matrix solution algorithm for the blunt nose and after body region by using a space marching technique. The integral matrix procedure enables us to create accurate and smooth results using the minimum grid in the boundary layer and to minimize the computational costs. This algorithm is highly appropriate for the design of hypersonic reentry vehicles. The effects of real gas on the flowfield characteristics are also studied in boundary layer solutions. Comparisons of the results with experimental data demonstrate that accurate solutions are obtained.

Keywords: Hypersonic flow; Equilibrium air; Boundary layer; Integral matrix method

Nomenclatures

ρ	Density
u,v	x and y direction velocity
k	Heat conductivity
h	Specific enthalpy
p	Static pressure
e	Specific internal energy
ξ, η	Tangential and normal coordinates in Computational domain
T	Static temperature
M_∞	Free stream Mach number
T_w	Wall temperature
R_N	Nose radios
s	Body surface length
r	Body radius
μ	Kinematic viscosity
Pr	Prandtl number
H	Total enthalpy
$\tilde{\gamma}$	Ratio of Specific heat
$\rho_{e,}$	Density on the edge of boundary layer
μ_e	Kinematic viscosity on the edge of boundary layer
u_e	Velocity magnitude on the edge of boundary layer
Re_∞	Free stream Reynolds number
T_∞	Free stream static temperature
J_{Max}	Maximum grid points
Q_∞	Free stream heat flux $=h_\infty \rho_\infty V_\infty$

Introduction

Hypersonic flows are very important for the design of high speed aircraft and reentry vehicles and some aerodynamic problems must be considered in this regard. Most of these problems arise because of extremely high flight altitudes, high flight velocities and high temperatures. The high temperatures and high convective velocities create an environment with significant effects of real gas. The accurate and efficient design of thermal protection systems, as well as propulsion systems for such vehicles will require accurate information of various aerothermodynamics environments. Since the aerothermodynamics environment for these flight conditions (high speeds and high temperatures) is extremely difficult to simulate in ground-based or flight experiments, the design process for these vehicles will be heavily based on the computational methods to define the aerothermodynamics environment during reentry.

1. Assistant Professor (Corresponding Author)
2. PhD Student

Received: 2014. 09. 20, Accepted: 2016. 01. 13

Several common computational approaches for obtaining accurate aerothermodynamics predictions of these vehicles are the Thin-Layer Navier-Stokes (TLNS) equations, the Parabolized Navier-Stokes (PNS) equations, the viscous shock layer (VSL) equations and the boundary layer equations. The numerical computations of hypersonic viscous flows using the TLNS equations especially for long slender blunt bodies are very time consuming and require very high storage and computer speed. Therefore, they are not well suited for various parametric studies needed for design and analysis processes.

Two approaches for the computation of high speed flows over slender-body supersonic/hypersonic geometries are the PNS or VSL equations. These equations are parabolic-like with respect to the stream-wise direction. The main difficulty in applying the PNS approach over blunt-body configurations is weakness of the PNS equations to solve the subsonic flowfield in the blunted nose, and therefore the TLNS equations must be used. The VSL equations are a more approximate set of equations than the PNS equations. In terms of complexity, they represent an intermediate level of approximation between the PNS equations and the boundary-layer equations. The VSL equations are also hyperbolic-parabolic in the stream wise direction so that a solution may be advanced downstream by using a spatial marching technique. Note that the solution of both the PNS and VSL schemes avoids the requirement to determine the second-order boundary-layer effects of vorticity and displacement thickness, and also matching the in viscid and viscous regions, required for the solution of the boundary-layer equations. The major drawback in use of the VSL equations for calculating hypersonic flows over blunt bodies is that they need starting solutions and an appropriate initial shock shape and also smoothing of intermediate shock shapes for the solution to be converged. In general, the VSL approaches are more sensitive to these values, and in the design environment such requirements of the user are undesirable.

A common alternative computational approach for obtaining accurate aerothermodynamics predictions of these vehicles is to use the equilibrium boundary layer (BL) equations. The BL equations are also parabolic-like with respect to the stream-wise direction; hence the BL scheme can realize appreciable decreases in both computational time and memory requirements relative to the other schemes like TLNS approximation method [1]. Based on this procedure a known code entitled “BLIMP” (Boundary Layer Implicit Method Procedure) developed in NASA [2].

Several researchers used a dual-code solution procedure (TLNS-PNS) or VSL to decrease the computational cost and develop an efficient procedure to predict the flowfield around hypersonic vehicles [3-8]. A TLNS solver is used in the nose region and a PNS solver for the after body region.

Such a solution strategy for computation of hypersonic flowfields over blunt-body geometries using two well-established TLNS and PNS codes, LAURA [9] and UPS [10]. These two codes were based on finite volume and shock capturing algorithms. The application of the dual-code solution procedure was shown for the solution of perfect gas, chemical equilibrium and chemical no equilibrium hypersonic flows about slender blunted cones. Esfahanian et al. [11] used a combined TLNS-PNS solution procedure for the blunt cone case.

The boundary layer equations have been used to efficiently solve the flowfield between the blunt bodies and in viscid region by some researcher using different algorithms [12, 13].

As mentioned before, high temperatures of air around the hypersonic vehicles create an environment where the real gas effects can be significant. This causes some errors in the numerical results when the perfect gas assumption is applied. Therefore, considering the real gas effects in high temperature flowfields seems necessary to create accurate results. Kamali [14] investigates the effects of equilibrium air for laminar and turbulent flow over the blunt bodies.

The main objective of the present work is to accurately and efficiently compute hypersonic laminar flows including equilibrium gas effects over reentry axisymmetric bodies. The numerical algorithms based on the integral matrix procedure with Taylor's series using the Newoton-Raphson's linearization can provide accurate and smooth solutions for geometries with small axial geometric variation. This procedure enables us to create accurate results using the minimum grid in the boundary layer and to minimize the computational costs. The effects of real gas on the flowfield characteristics are also studied in boundary layer solutions.

To demonstrate the accuracy and efficiency of using the present algorithm, two computations are performed for hypersonic flows over blunt-bodies. The present computations are performed for hypersonic flow over two long slender blunt cones at Mach number of 19.25 and 6.89 and over a sphere at Mach number of 11.26. The results of these computations are compared with available numerical and experimental results. For the above calculations, the perfect gas solutions are also performed and some details on the treatment of real gas effects on the flowfield characteristics are provided.

Problem Formulations

The PDEs for a compressible laminar boundary layer which express the conservation of mass, momentum and energy can be written as follows:

$$\frac{\partial}{\partial x}(\rho u r^j) + \frac{\partial}{\partial y}(\rho v r^j) = 0 \qquad (1)$$

$$\rho u\frac{\partial u}{\partial x}+\rho v\frac{\partial u}{\partial y}=-\frac{\partial P}{\partial x}+\frac{1}{r^j}\frac{\partial}{\partial y}\left(\mu r^j\frac{\partial u}{\partial y}\right) \quad (2)$$

$$\frac{\partial p}{\partial y}=0 \quad (3)$$

$$\rho u\frac{\partial H}{\partial x}+\rho v\frac{\partial H}{\partial y}=\frac{1}{r^j}\frac{\partial}{\partial y}\left(\frac{\mu}{Pr}r^j\frac{\partial H}{\partial y}\right)+\frac{1}{r^j}\frac{\partial}{\partial y}\left(\mu\left(1-\frac{1}{pr}\right)r^j\frac{\partial}{\partial y}\left(\frac{u^2}{2}\right)\right) \quad (4)$$

Where r is body curvature radius, (x,y) are the tangential and normal directions, (u , v)are the corresponding velocity components in directions (x ,y), ρ, p and H are the density, pressure and total enthalpy, respectively. μ and Pr are the fluid viscosity and prandtl number. 2D or axisymmetric equations can be used by selecting $j=0$ or $j=1$. The physical coordinate system (x,y) can be transformed to a computational coordinate system (ξ,η). The common levy-lees transformation can be written as follows [9]:

$$\xi(x)=\int_0^x \rho_e\mu_e u_e r_b^{2j}\,dx \quad (5)$$

$$\eta(x,y)=u_e(2\xi)^{-1/2}\int_0^y \rho r^j\,dy \quad (6)$$

Thus, the transformed stream-wise momentum and energy equations can be written in the forms:

$$\frac{\partial}{\partial\eta}\left(N\frac{\partial^2 f}{\partial\eta^2}\right)+f\frac{\partial^2 f}{\partial\eta^2}+2\frac{\xi}{u_e}\frac{du_e}{d\xi}\left(\frac{\rho_e}{\rho}-\left(\frac{\partial f}{\partial\eta}\right)^2\right)=2\xi\left(\frac{\partial f}{\partial\eta}\frac{\partial^2 f}{\partial\xi\partial\eta}-\frac{\partial f}{\partial\xi}\frac{\partial^2 f}{\partial\eta^2}\right) \quad (7)$$

$$\frac{\partial}{\partial\eta}\left(\frac{N}{Pr}\frac{\partial g}{\partial\eta}\right)+f\frac{\partial g}{\partial\eta}+\frac{u_e^2}{H_e}\frac{\partial}{\partial\eta}\left(N\left(1-\frac{1}{Pr}\right)\frac{\partial f}{\partial\eta}\frac{\partial^2 f}{\partial\eta^2}\right)=2\xi\left(\frac{\partial f}{\partial\eta}\frac{\partial g}{\partial\xi}-\frac{\partial f}{\partial\xi}\frac{\partial g}{\partial\eta}\right) \quad (8)$$

where $N=\frac{\rho\mu}{\rho_e\mu_e}$, $g=\frac{H}{H_e}$ and $f=\frac{u}{u_e}$. To "close" the preceding system of equations, relations between the thermodynamic variables are required along with relations for the transport properties μ and k. As it is known, the pressure is approximately constant across the boundary layer. For the equilibrium air, the relation between the pressure, density and temperature (state equation) can be written as:

$$p=\rho h\frac{\tilde{\gamma}-1}{\tilde{\gamma}} \quad (9)$$

For the equilibrium gas, the ratio of specific heats $(\tilde{\gamma})$ is the function of the pressure and density:

$$\tilde{\gamma}=\tilde{\gamma}(\rho,p) \quad (10)$$

There are some approximate curve fits for the equilibrium air [15, 16] which give the relations between the thermodynamic properties. In the present equilibrium flow computations, the ratio of specific heats $(\tilde{\gamma}(\rho,p))$ and the other thermodynamic properties are obtained using the correlations developed by Srinivasan et al. [16].

$$h=h(\rho,p),\quad T=T(\rho,p) \quad (11)$$

These curve fits are valid for temperatures up to 25000 K and density ratios (ρ/ρ_0) from 10^{-7} to 10^3. The curve fits for the transport properties were developed by Srinivasan et al. [17] and include the following correlations:

$$\mu=\mu(\rho,T),\ k=k(\rho,e),\ Pr=Pr(\rho,T) \quad (12)$$

These curve fits are valid for temperatures up to 15000 K and the density ratios (ρ/ρ_0) from 10^{-5} to 10^3.

For both the equilibrium air and the perfect gas, the following relations between flow variables can be used [15, 16]:

$$p=\rho e(\tilde{\gamma}-1),\quad E=\rho\left[e+\frac{V^2}{2}\right],\quad \tilde{\gamma}=\frac{h}{e} \quad (13)$$

For the perfect gas computations, $\tilde{\gamma}=\gamma_\infty=1.4$, the molecular viscosity $\mu$is determined by the Sutherland law and the coefficient of thermal conductivity K is calculated by assuming a constant Prandt l number, Pr= 0.72.

Integral Matrix Procedure

The basis of the integral matrix algorithm is integration of the momentum and the energy equations at constant ξ between two points (j-1 and j) across the boundary layer:

$$(Nf'')_{j-1}^{j}+\int_{j-1}^{j} f f''d\eta+\beta\int_{j-1}^{j}\frac{\rho_e}{\rho}d\eta-\beta\int_{j-1}^{j} f'^2\,d\eta=\int_{j-1}^{j}2\left(f'\frac{\partial f'}{\partial(ln\xi)}-f''\frac{\partial f}{\partial(ln\xi)}\right)d\eta \quad (14)$$

$$\left(\frac{N}{Pr}g'\right)_{j-1}^{j}+\frac{u_e^2}{H_e}\left(N\left(1-\frac{1}{Pr}\right)f'f''\right)_{j-1}^{j}+\int_{j-1}^{j} f\,g'd\eta=\int_{j-1}^{j}2\left(f'\frac{\partial g}{\partial(ln\xi)}-g'\frac{\partial f}{\partial(ln\xi)}\right)d\eta \quad (15)$$

All terms of the momentum and energy equations are discredited by Taylors series. Finally, the momentum and energy equation can be simplified as:

$$\begin{aligned}&\left[Nf''+f'\left((1+d_0)f_i+d_1f_{i-1}+d_2f_{i-2}\right)\right]_{j-1}^{j}+\\&\beta\left[\left(\frac{\rho_e}{\rho_j}+\frac{\rho_e}{\rho_{j-1}}\right)\frac{\delta\eta}{2}+\left(\frac{\rho_e\rho'_j}{\rho_j^2}+\frac{\rho_e\rho'_{j-1}}{\rho_{j-1}^2}\right)\frac{\delta\eta^2}{12}\right]-\\&(1+\beta+2d_0)\left[f'_j\,XP_1+f''_j\,XP_2+f'''_j\,XP_3+f'''_{j-1}\,XP_4\right]-2\left[f'_j\,ZP_1+f''_j\,ZP_2+f'''_j\,ZP_3+f'''_{j-1}\,ZP_4\right]=0\end{aligned} \quad (16)$$

$$\begin{aligned}&\left[\left(\frac{N}{Pr}g'\right)+\frac{u_e^2}{H_e}\left(N\left(1-\frac{1}{Pr}\right)f'f''\right)\right]_{j-1}^{j}+\\&\left[g\left((1+d_0)f_i+d_1f_{i-1}+d_2f_{i-2}\right)\right]_{j-1}^{j}\\&=(1+2d_0)\left[f'_j\,XP_1+f''_j\,XP_2+f'''_j\,XP_3+\right.\end{aligned} \quad (17)$$

$$f'''_{j-1} XP_4\Big]_{p_j=g_j} + \Big[f'_j ZP_1 + f''_j ZP_2 + f'''_j ZP_3 + f'''_{j-1} ZP_4\Big]_{p_j=g_j} + \Big[g_j ZP_1 + g'_j ZP_2 + g''_j ZP_3 + g''_{j-1} ZP_4\Big]_{p_j=f'_j}$$

Where,

$$XP_1 = \delta\eta\left(P_j - P'_j\frac{\delta\eta}{2} + P''_j\frac{\delta\eta^2}{8} + P'''_{j-1}\frac{\delta\eta^2}{24}\right) \quad (18)$$

$$XP_2 = -\delta\eta^2\left(\frac{P_j}{2} - P'_j\frac{\delta\eta}{3} + P''_j\frac{11\delta\eta^2}{120} + P'''_{j-1}\frac{\delta\eta^2}{30}\right) \quad (19)$$

$$XP_3 = \delta\eta^3\left(\frac{P_j}{8} - P'_j\frac{\delta\eta}{120} + P''_j\frac{11\delta\eta^2}{420} + P'''_{j-1}\frac{5\delta\eta^2}{504}\right) \quad (20)$$

$$XP_4 = \delta\eta^3\left(\frac{P_j}{24} - P'_j\frac{\delta\eta}{30} + P''_j\frac{5\delta\eta^2}{504} + P'''_{j-1}\frac{\delta\eta^2}{252}\right) \quad (21)$$

and

$$ZP_1 = \delta\eta\left(YP_1 - YP'_2\frac{\delta\eta}{2} + YP_3\frac{\delta\eta^2}{8} + YP_4\frac{\delta\eta^2}{24}\right) \quad (22)$$

$$ZP_2 = -\delta\eta^2\left(\frac{YP_1}{2} - YP_2\frac{\delta\eta}{3} + YP_3\frac{11\delta\eta^2}{120} + YP_4\frac{\delta\eta^2}{30}\right) \quad (23)$$

$$ZP_3 = \delta\eta^3\left(\frac{YP_1}{8} - YP_2\frac{\delta\eta}{120} + YP_3\frac{11\delta\eta^2}{420} + YP_4\frac{5\delta\eta^2}{504}\right) \quad (24)$$

$$ZP_4 = \delta\eta^3\left(\frac{YP_1}{24} - YP_2\frac{\delta\eta}{30} + YP_3\frac{5\delta\eta^2}{504} + YP_4\frac{\delta\eta^2}{252}\right) \quad (25)$$

and

$$YP_1 = d_1P^j_{i-1} + d_2P^j_{i-2} \quad (26)$$

$$YP_2 = d_1P'^j_{i-1} + d_2P'^j_{i-2} \quad (27)$$

$$YP_3 = d_1P''^j_{i-1} + d_2P''^j_{i-2} \quad (28)$$

$$YP_4 = d_1P''^{j-1}_{i-1} + d_2P''^{j-1}_{i-2} \quad (29)$$

d_0, d_1 and d_2 can be calculated by two or three points backward discrimination [2]. Equations (16) and (17) are linear zed by Newoton-Raphson's method. To close the system of equations, five Taylor's series for f ،f′ ،f′′،g and g′ can be used. The system of equations is implicitly solved for each step and supply the necessary information for the next step. Using this algorithm, the entire boundary flowfield can be solved by space marching technique.

Boundary Conditions and Initial Data

The boundary conditions at the wall consist of no-slip conditions for velocity components ($u = v = 0$), a specified wall temperature or an adiabatic wall. For a perfect gas, the density at the wall is determined using the perfect gas relation. For a real gas, the wall density is calculated implicitly from the curve fit expression, T = T (ρ,p). At the upper boundary, the in viscid flow properties which include the velocity, pressure and temperature of the edge of boundary layer are applied. These properties are calculated from in viscid flowfield solution. It is noted that the in viscid solver must be also set for equilibrium air when the boundary layer is solved by equilibrium assumption (see Figure 1). Starting data of the boundary layer equations in the stagnation point of the blunt geometries are provided by the similar Hiemenz solution.

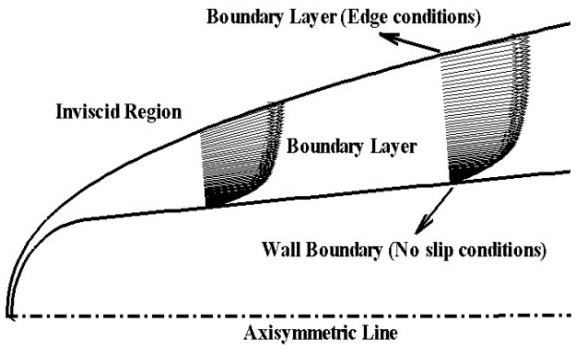

Fig. 1. Schematic of boundary conditions

Results and Discussion

Test case 1

The first test case is hypersonic laminar flow of equilibrium air over a long slender blunted cone. The flow conditions for this test case correspond to the Reentry-F flight altitude of 36.576 km [18]. The Reentry-F configuration is 5^0 half angle sphere-cone with an overall length of 3.962 m and an initial nose radius of $R_N = 0.29$ cm. The flow conditions are:

$M_\infty = 19.25, \quad Re_\infty = 7570.4$

$T_\infty = 243$ K, $\quad T_w = 361 - 477$ K

This is a challenging case to compute high Mach number flow over such a large scale model. The present boundary layer approach is applied to this case to show the efficiency and accuracy of the proposed method and to study the effects of real gas for long blunt-body geometry. The present method needs the conditions of boundary layer edge for equilibrium air. These data are provided by an in viscid equilibrium code. Figure 2 indicates the no dimensional pressure contours around this geometry for equilibrium air. The pressure reference is the infinity pressure. It is noted that the pressure is approximately constant across the boundary layer. Figures 3 to 5 show the distribution of the corresponding surface pressure, velocity and temperature for in viscid solution of equilibrium air. These conditions are applied as upper boundaries for the solution of boundary layer equations. As show in Figs. 3 and 5, there is an expansion zone near the blunt nose. In fact, conversion of a strong bow shock to an oblique shock near the nose needs a strong expansion and causes strong pressure and temperature decrease.

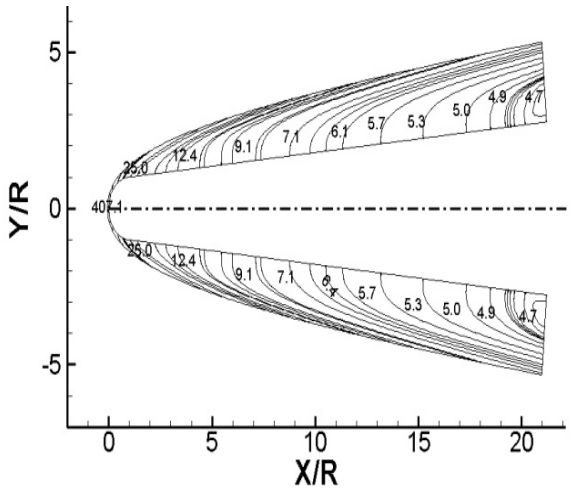

Fig. 2. Pressure contours for 5^0 blunt cone, $\mathbf{M_\infty = 19.25}$

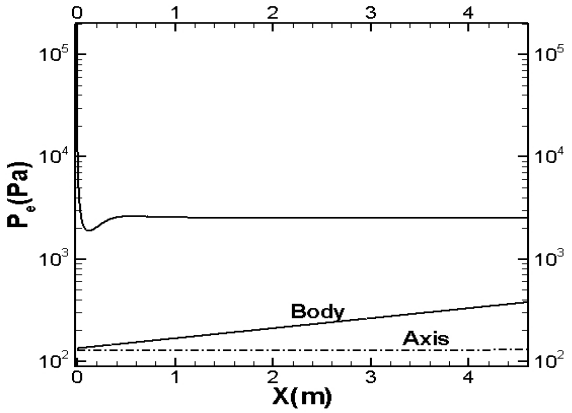

Fig. 3. Surface pressure distribution for 5^0 blunt cone, $M_\infty = 19.25$

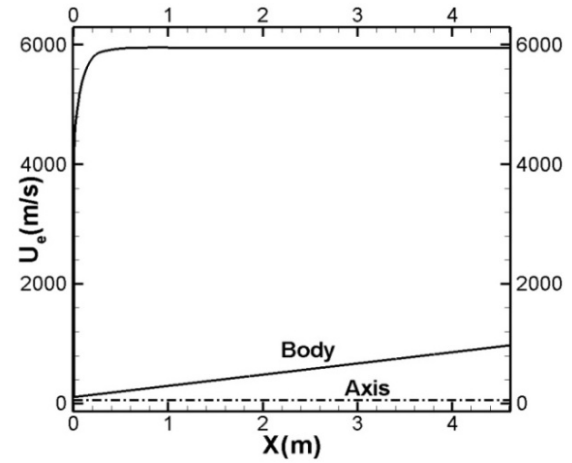

Fig. 4. Velocity distribution of boundary layer edge for 5^0 blunt cone, $M_\infty = 19.25$

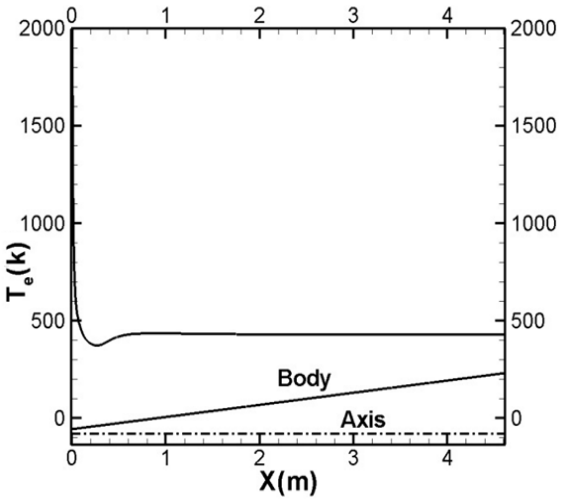

Fig. 5. Temperature distribution of boundary layer edge for 5^0 blunt cone, $M_\infty = 19.25$

The grid distribution and the velocity profiles in the boundary layer are shown in Figure 6. The maximum number of grid used for this solution is $J_{Max} = 10$ and the maximum η is about 2.75. In this case, grid study isperformed for the surface heating rates on the wall by $J_{Max} = 10, 15$ and 55 (see Figure 7). It is observed that results captured by less than 10 points in the boundary layer have some oscillations and errors. Thus, 15 points in the boundary layer are enough for predicting appropriate results. Comparison of the surface heating rates computed by the present technique by $J_{Max} = 15$ with the experimental Reentry-F flight data and the result for the perfect gas is shown in Figure8. The Reentry-F flight experiment involved the accurate measurement of surface heating rates on a long slender conical RV under laminar flow conditions. The results of the present solution are found to be in a better agreement with the experimental data. The results show the surface heating rates for the equilibrium air are higher than those of the perfect gas up to about 18%. This may be because of decrease of the boundary layer thickness due to the real gas effects. Figure 9 compares the computed skin friction coefficient distribution for the solutions with the equilibrium and perfect gas assumption. It is observed that the skin friction coefficient, rather than the perfect gas, is increased when the equilibrium air is used for simulation. By comparing the viscosity coefficient between the perfect gas and the equilibrium air, it is found that the calculated viscosity from the curve fits ($\mu = \mu(\rho, T)$) for the equilibrium model ishigher than that of the perfect model ($\mu = \mu(\rho, T)$). This also causes higher velocity gradient and thus higher skin friction coefficient in comparison with the perfect model.

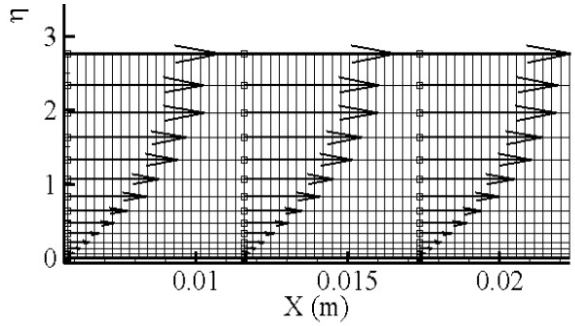

Fig. 6. Grid distribution and velocity vectors for 5^0 blunt cone, $M_\infty = 19.25$

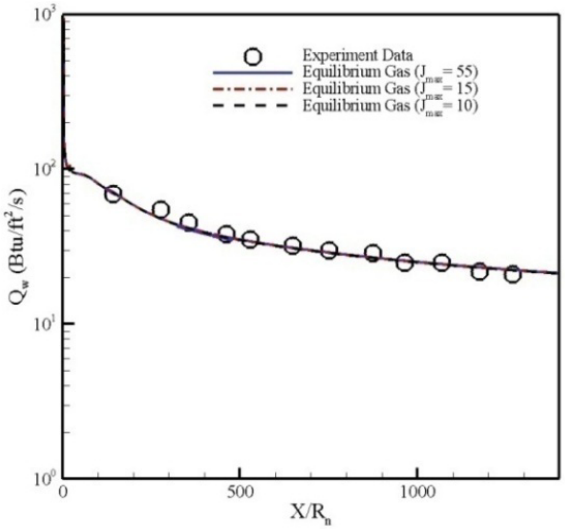

Fig. 7. Grid study of the surface heating rates for 5^0 blunt cone, $M_\infty = 19.25$

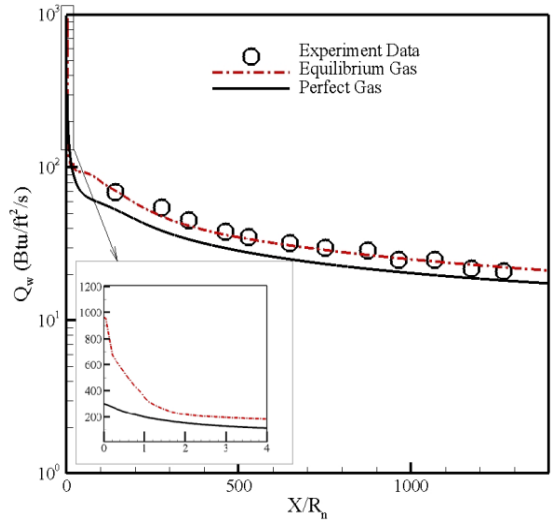

Fig. 8. Comparison of the surface heating rates for 5^0 blunt cone, $M_\infty = 19.25$

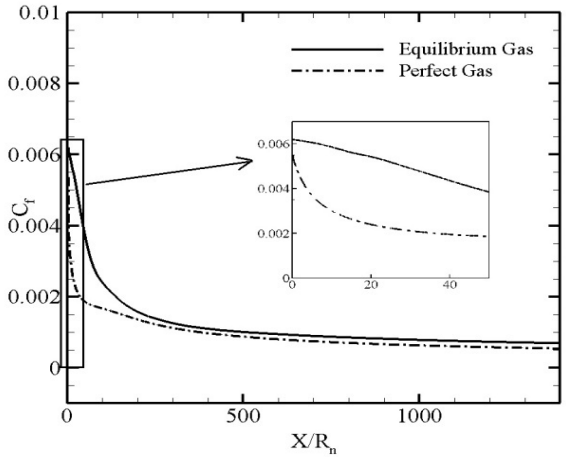

Fig. 9. Comparison of the skin friction coefficient for 5^0 blunt cone, $M_\infty = 19.25$

For the equilibrium airflow computation, the typical CPU time of the boundary layer solution, using 10 grid points in the wall normal direction and 15000 sweeps in the stream-wise direction is about 90 seconds. It is clear that the present boundary layer solution strategy significantly reduces the computer time and storage required to obtain the equilibrium hypersonic flowfield with a reasonable accuracy.

Test case 2

The second test case computed is hypersonic laminar flow of equilibrium air over a 12.84^0 half angle bicone. The nose radius for this case is $R_N = 0.29$ m. This test case was tested in NASA Langley Expansion-Tube Facility [14]. The flow conditions are:

$M_\infty = 6.89, \quad Re_\infty = 1695,$
$T_\infty = 1604$ K, $\quad T_w = 302 - 388$ K

This test case is used to study the high temperature effects and shows the efficiency and accuracy of the present code. Fully laminar flow conditions are assumed and both the perfect and equilibrium airflow computations are performed. Figures 10 and 11 indicate the no dimensional pressure contour and distribution of the surface pressure for in viscid solution around this geometry. Distribution of the surface temperature for in viscid solution is shown in figure 12. These data are applied as conditions at upper boundaries of the boundary layer equations. The grid distribution in the boundary layer is shown in figure 13. The maximum number of grid used for this solution is $J_{Max} = 10$ and the maximum η is about 3.1. In this case, grid study is also performed for the surface heating rates on the wall by $J_{Max} = 5, 10$ and 28 (see Fig. 14). It is observed that 10 points in the boundary layer are enough for predicting appropriate results.

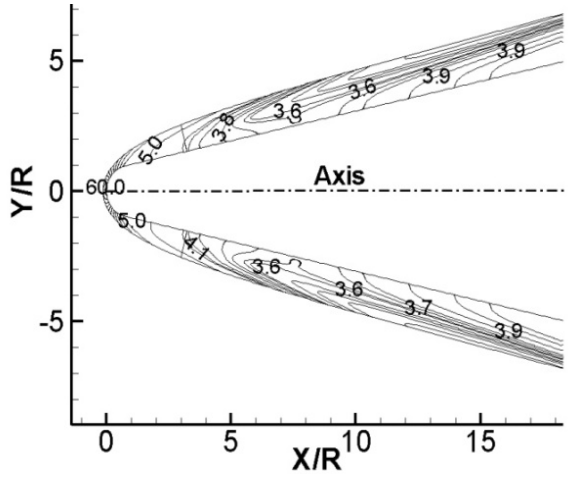

Fig. 10. Pressure contours for 12.84^0 blunt cone, $M_\infty = 6.89$

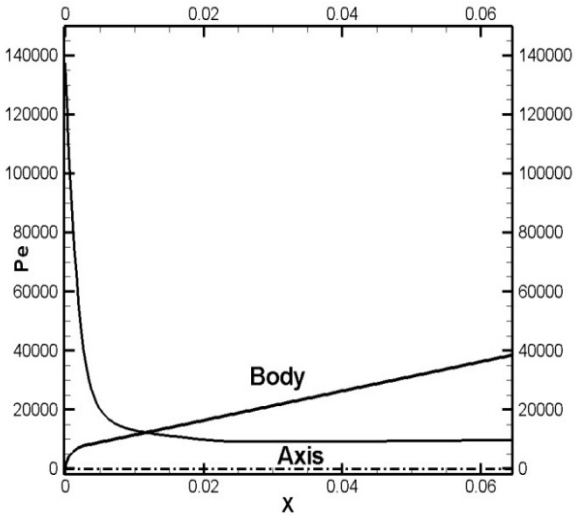

Fig. 11. Surface pressure distribution for 12.84^0 blunt cone, $M_\infty = 6.89$

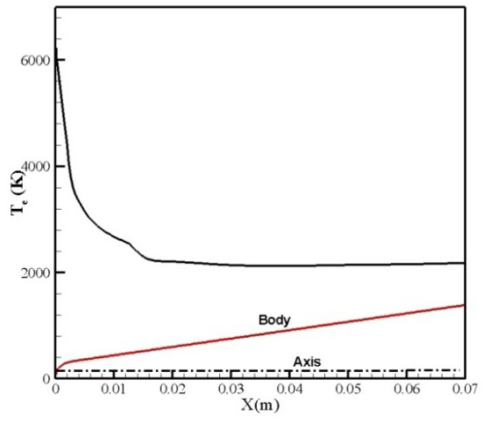

Fig. 12. Temperature distribution of boundary layer edge for 12.84^0 blunt cone, $M_\infty = 6.89$

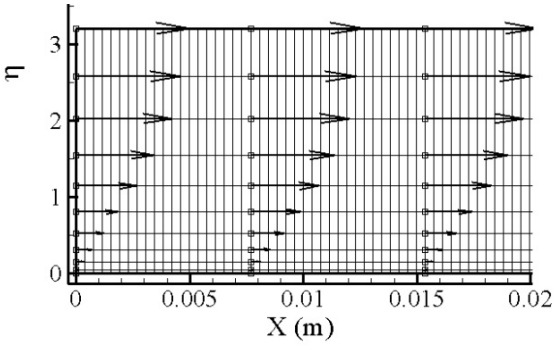

Fig. 13. Grid and velocity vectors for 12.84^0 blunt cone, $M_\infty = 6.89$

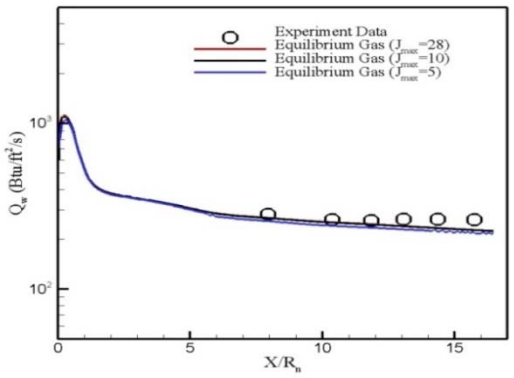

Fig. 14. Grid study of the surface heating rates for 12.84^0 blunt cone, $M_\infty = 6.89$

Figure 15, compares the results of the surface heating rates from the present code with the experiment [19]. The present computations are performed for both the perfect and equilibrium airflows. The results show that the perfect-gas model underestimate the wall heat-transfer rates about 12%. The present predictions of the equilibrium air are in better agreement with the experimental data. In this case, the CPU time of the boundary layer solution, using 10 grid points in the wall normal direction and 175 sweeps in the stream wise direction, is less than 10 sec with a reasonable accuracy.

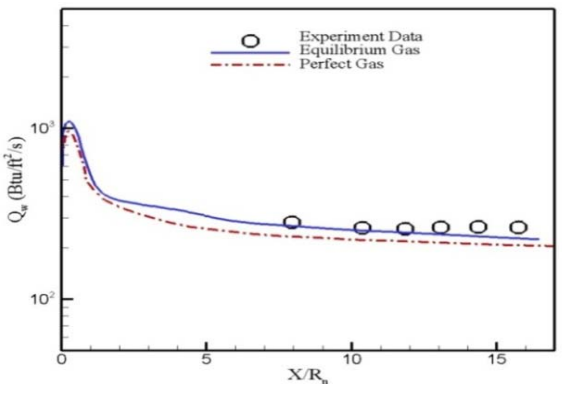

Fig. 15. The surface heating rates for 12.84^0 blunt cone, $M_\infty = 6.89$

Test case 3

To investigate the results near the stagnation region, the third test case is performed for hypersonic laminar flow of equilibrium air over a sphere with nose radius of $R_N = 0.25$ m. The flow conditions are

$M_\infty = 11.26, \quad Re_\infty = 4976.16$
$T_\infty = 182.33$ K, $\quad T_w = 1000$ K

This condition is according to flight data at 250,000 ft height and velocity 10,000 ft/s. Distribution of the surface temperature, pressure and velocity for in viscid solution are shown in figure 16. These data are applied as conditions at upper boundaries of boundary layer equations. The maximum number of grid used for this solution is $J_{Max} = 15$ and the maximum η is about 2.9. Fig. 17 compares the results of the surface heating rates from the present code with the numerical results of Ref. [14] which are created by the second order finite difference Beam-Warming method and shock fitting algorithm. The present predictions of the equilibrium air near the stagnation region are in good agreement with this numerical result.

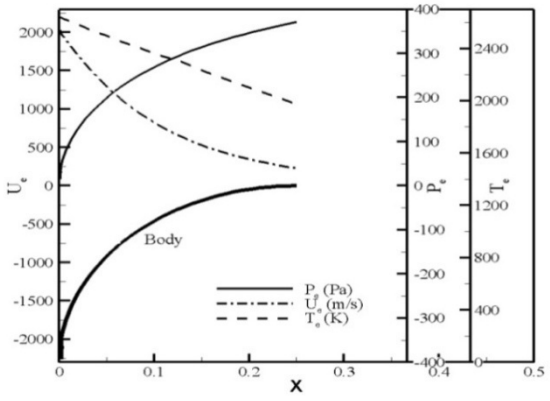

Fig. 16. Surface pressure, temperature and velocity distribution for sphere$M_\infty = 11.26$

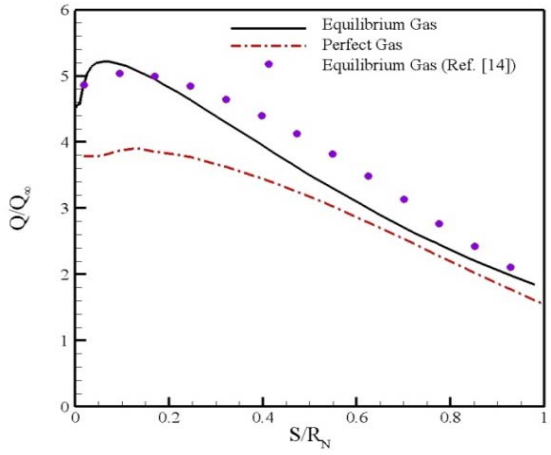

Fig. 17. The surface heating rates for sphere, $M_\infty = 11.26$

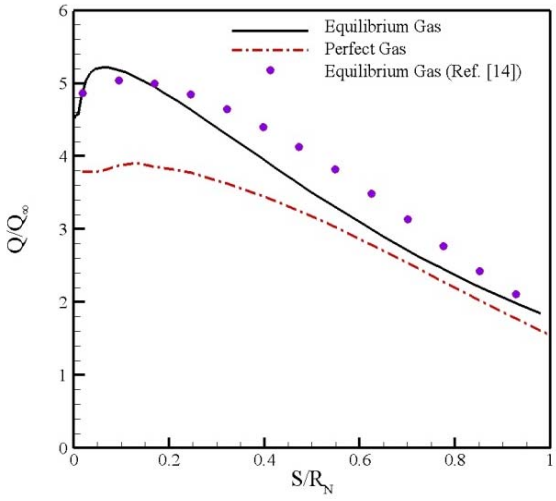

Fig. 18. The surface heating rates for sphere, $M_\infty = 11.26$

Conclusions

In the present work an accurate and efficient computational procedure is developed to predict the laminar hypersonic flowfield for both the perfect gas and equilibrium air around the axisymmetric blunt body configurations. The numerical algorithms based on the integral matrix procedure with Taylor's series using the Newton-Raphson's linearization can provide accurate and smooth solutions for blunt nose and after-body region. Using a space marching technique and the integral matrix procedure enable us to create accurate and smooth results using the minimum grid in the boundary layer and to minimize the computational costs. This algorithm is highly appropriate for the design of hypersonic reentry vehicles. To demonstrate the accuracy and efficiency of using the present algorithm, two computations are performed for hypersonic flows over blunt-bodies. Comparison of the results, especially heating rate on the body surface, between perfect gas and equilibrium air is performed for three cases and the effects of real gas on the flowfield characteristics are also studied in the boundary layer solutions. The results of these computations are compared with available numerical and experimental results. Comparisons of the results with experimental data demonstrate that higher and more accurate solutions are obtained by equilibrium assumption as compared with the perfect gas.

References

[1] Shlichting, H. and Gersten, K., *Boundary-Layer Theory*, Springer, New York, 2000.

[2] Bartlett E.P. and Kendall R.M., *Nonsimilar Solution of the Multicomponent Laminar Boundary Layer by an Integral Matrix Method*, NASA CR-1062, Part III, 1967.

[3] Wood, W.A., Eberhardt, S., "Dual-code Solution Strategy for Chemically Reacting Hypersonic Flows," *33rd Aerospace Sciences Meeting and Exhibit, Aerospace Sciences Meetings (AIAA Paper),* 1995, pp.95-0158.

[4] Wood, W.A., Thompson, R.A. and Eberhardt, S., "Dual-Code Solution Strategy for Hypersonic Fows," *Journal of Spacecraft and Rockets,* Vol. 33, No. 3, 1995, pp. 449–451.
[5] Hejranfar, K., Kamali-Moghadam, R. and Esfahanian, V., "Dual-code Solution Procedure for Efficient Computing Equilibrium Hypersonic Axisymmetric Laminar Flows," *Aerospace Science and Technology,* Vol. 12, Issue 2, 2008, pp. 135–149,
[6] Thompson R.A., Zoby E.V., Wurster K.E. and Gnoffo P.A., An Aero Thermodynamic Study of Slender Conical Vehicles, *AIAA Paper* 87-1475, 1987.
[7] Cheatwood, F.M. and Dejarnette, F.R., "Approximate Viscous Shock Layer Technique for Calculating Hypersonic Flows About Blunt-Nosed Bodies," *Journal of Spacecraft and Rockets*, Vol. 31, No. 4, 1994, pp. 621-629.
[8] Noori S., Ghasemloo S. and Mani M., "A New Method for Solution of Viscousshock-Layer Equations," *Proceeding of the Institution of Mechanical Engineers Part G-Journal of Aerospace Engineering*, Vol. 224, No.1, 2008, pp.719-729,.
[9] Gnoffo, P.A., Gupta, R.N. and Shinn, J.L., Conservation Equations and Physical Models for Hypersonic Air Flows in Thermal and Chemical Non-equilibrium, NASA TP 2867, 1989.
[10] Buelow, P.E., Tannehill, J.C., Ievalts, J.O. and Lawrence, L.S., "Three Dimensional, Upwind, Parabolized Navier–Stokes Code for Chemically Reacting Flows," *Journal of Thermophysics and Heat Transfer*, Vol. 5, No. 3, 1991, pp. 274–283.
[11]Esfahanian, V. and Hejranfar, K., Accuracy of parabolized Navier–Stokes Schemes for Stability Analysis of Hypersonic Axisymmetric Flows, *AIAA Journal,* Vol. 40, No. 7, 2002, pp. 1311–1322.
[12]Kendall, R. M., Bartlett, E. P., Rindall, R. A. and Moyer, C.B., "An Analysis of Chemically Reacting Boundary Layer," Issued by Originator as Aerotherm Report No. 66-7, Part 1, 1961.
[13] Kopriva, D.A., "Spectral Solution of the Viscous Blunt Body Problem II: Multidomain Approximation," ICASE Report No. 94-73, 1994.
[14] Kamali-Moghadam R., Dual-code TLNS-PNS Solution Procedure for Efficient Computing Equilibrium Hypersonic Axisymmetric Flows, (M.Sc. Thesis), The Sharif University of Technology, Tehran, Iran, December 2005.
[15] Tannehill, J.C. and Mugge, T.L., "Improved Curve-Fits for the Thermodynamic Properties of Equilibrium Air Suitable for Numerical Computation Using Time Dependent or Shock-Capturing Methods, NASA CR-2470, 1974.
[16] Srinivasan, S., Tannehill, J.C. and Weilmuenster, K.J., *Simplified Curve Fits for the Thermodynamic Properties of Equilibrium Air*, NASA RP-1-313, 1986.
[17] Srinivasan, S., Tannehill, J.C. and Weilmuenster, K.J., *Simplified Curve Fits for the Transport Properties of Equilibrium Air*, NASA RP-1181, 1987.
[18] Bhutta, B.A. and Lewis, C.H., "Comparison of Hypersonic Experiments and PNS Predictions, Part I: Aerothermodynamics," *Journal of Spacecraft and Rockets,* Vol. 28, No. 4, 1991, pp. 376-386.
[19] Miller, C.G., Micol, J.R. and Gnoffo, P.A., Laminar Heat-Transfer Distribution on Biconics at Incidence in Hypersonic-Hypervelocity Flows, NASA, TP-2213, 1985.